Shifting seasons: Long-term crop dynamics across agroclimatic regions of Czechia

Jiří Tomíček[1,2], Jan Mišurec[2], Markéta Potůčková[1,*]

[1] Charles University, Faculty of Science, Department of Applied Geoinformatics and Cartography, Czechia
[2] Gisat Ltd., Czechia
[*] Corresponding author: marketa.potuckova@natur.cuni.cz

ABSTRACT

This study analyzes the evolution of phenological (start-of-season, end-of-season, length-of-season, day of maximum-of-season) and productivity (small and large seasonal integrals) parameters for six major crop types in Czechia (winter cereals, spring cereals, winter rapeseed, fodder crops, sugar beetroot, and corn), using a 35-year Landsat time series (1986–2020). The leaf area index (LAI) was retrieved using an artificial neural network regression model trained on PROSAIL radiative transfer simulations and validated with extensive in situ measurements collected in 2017 and 2018 in the lowlands of Central Bohemia. The supervised classification of Landsat quarterly composites enabled the identification of crop spatial patterns for each growing season. Phenological and productivity indicators were then derived from LAI time series aggregated at the level of ten agro-climatic regions using the threshold approach. Changes in phenological and productivity parameters over the examined period were assessed through the linear least squares regression analysis and the significance of trends was tested. Results revealed significant negative trends in the end-of-season and day of maximum-of-season for winter and spring cereals, winter rapeseed (up to –0.7 days/year), and fodder crops (up to –1.6 days/year), indicating an earlier maturation and harvest. Significant differences in trends in phenological and productivity parameters were observed between agro-climatic regions in more than 40% of cases, and the response was observed to be highly crop-specific. While the shift in harvest dates and the shortening of the season for corn and fodder crops were more pronounced in warmer regions, the shift in winter rapeseed phenology occurred more rapidly in colder regions. The findings underscore the relevance of crop type and regional climate in shaping phenological responses, offering a basis for future research and planning of agricultural adaptation strategies.

KEYWORDS

Landsat; leaf area index; PROSAIL; land surface phenology; productivity; Czechia

Received: 20 June 2025
Accepted: 8 October 2025
Published online: 27 November 2025

Tomíček, J., Mišurec, J., Potůčková, M. (2025): Shifting seasons: Long-term crop dynamics across agroclimatic regions of Czechia. AUC Geographica 60(2), 233–253
https://doi.org/10.14712/23361980.2025.22
© 2025 The Authors. This is an open-access article distributed under the terms of the Creative Commons Attribution License (http://creativecommons.org/licenses/by/4.0).

1. Introduction

Phenology studies periodic life cycles of living organisms in relation to weather, climate or other biotic and abiotic factors (Lieth 1974; Nord and Lynch 2009). It is mostly based on monitoring time occurrence of certain clearly recognizable signs of plant development (i.e. emergence, flowering, changes in coloring, etc.), which are generally known as "phenological events". The periods between them are then referred as "phenological phases (Caparros-Santiago et al. 2021). The shifts of phenological events due to climate change have been foreseen and studied for decades (Sparks and Carey 1995; Menzel 2000; Hassan et al. 2023). In the case of plants, the most evident are advancements in spring and summer but delay in autumn (Caparros-Santiago et al. 2021; Hassan et al. 2023; Campioli et al. 2025). An increasing length of the growing season on one hand causes an increase in net primary production but on the other hand has impacts on atmospheric CO2 content (positive in spring time, negative due to extending autumn phenophases), water exchange or alternation in species interaction which may cause a decrease of biodiversity (Caparros-Santiago et al. 2021; Yuan et al. 2024).

The ground phenological (GP) observations have a long history (Koch et al. 2007; Hajkova et al. 2012; Fitchett et al. 2015). Standardized procedures have been developed to date. Thus, the phenological data can be collected by volunteers in order to obtain higher spatial coverage (Kaspar et al. 2014). In spite of these efforts, the number of measurements is limited both in time and space. Satellite based monitoring of vegetation growth stages, known as Land Surface Phenology (LSP), allows for much larger spatial scale using time series of vegetation-related characteristics derived from the multispectral imagery (Caparros-Santiago et al. 2021; Gašparović et al. 2024). Unlike GP, LSP does not determine the phenological events based on the presence of specific signs of plant development. Instead, it defines the date on which a certain level of the vegetation-related characteristics under consideration is achieved by observing the vegetation cover (e.g., the date on which the maximum value of a given vegetation-related indicator is reached in a given year). LSP brings advantages, such as being cost-effective and easier to relate to climatic measurements that are usually coarser in resolution and might be difficult to fit GP observations. However, LSP is also affected by noise caused by sensor and processing flaws, or mixed signals from multiple land covers. It is also better suited to community-based than individual-based observations. It is common practice to combine GP and LSP observations when GP serves as the ground truth for deriving and testing LSP models, and when LSP is used to upscale GP observations (Rodriguez-Galiano et al. 2015).

Phenological observations have long received attention in agriculture (Wielgolaski 1974; Chmielewski 2013). They are essential for crop management (e.g., efficient irrigation, fertilization, pest management), yield estimation, or controlling crop agricultural policies (Meroni et al. 2021; Pei et al. 2025). Satellite data with a wide range of spectral, spatial, and temporal resolutions is used for crop phenology mapping (Gao and Zhang 2021). The sensors on the Landsat satellites provide long-term data with high spatial (30 m) and temporal (16 days) resolution. In addition to the spatial resolution of 10 or 20 m, the Sentinel 2 MSI sensor offers a higher temporal resolution (up to 5 days) thanks to the constellation of two satellites. Compared to Landsat data, it also has additional red-edge and SWIR spectral bands suitable for vegetation monitoring. As a result, both Landsat and Sentinel data, as well as their harmonized products (HLS) (Claverie et al. 2018), are among the most widely used for monitoring agricultural crops at regional or higher levels (Chaves et al. 2020; Misra et al. 2020; Gao and Zhang 2021; Htitiou et al. 2024). They can be fused with lower spatial but higher temporal resolution data, such as Moderate Resolution Imaging Spectroradiometer (MODIS) or Advanced Baseline Imager (ABI) to densify the time series for modeling crop grows in near real time (Schreier et al. 2021; Sisheber et al. 2022; Dhillon et al. 2023; Shen et al. 2023). Some authors have attempted to solve the problem of clouds in optical data by fusion with SAR data. Meroni et al. (2021) showed the complementarity of Sentinel-1 and Sentinel-2 data for LSP retrieval, especially for winter crops.

Key LPS parameters derived from satellite images include start of the season (SOS), end of the season (EOS), length of the season (LOS), peak of the season (POS), mild greenup and mild greendown (Hanes et al. 2014). The common way to determine them is to apply curve-based or trend-based approaches to the generated time series of the selected vegetation index (VI) such as normalized differential vegetation index (NDVI), enhanced vegetation index (EVI), or leaf area index (LAI). Curve-based approaches fit phenological curves derived from historical time series of VIs to current observations to predict current and future crop growth stages. They are robust and reliable for crops with consistent growth cycles. Trend-based approaches detect upward or downward trends from current time series data using momentum and VI thresholds. They are simpler to implement and more flexible to unexpected changes in crop growth patterns. However, they are less effective for forecasting future phenological stages and are more susceptible to noise and anomalies in the data (Eklundh and Jönsson 2016; Gao and Zhang 2021). Based on VI time series and LSP parameters, crop biomass (Dong et al. 2020), gross and net primary production (Gitelson et al. 2012), or yield (Skakun et al. 2019; dos Santos Luciano et al. 2021; Dhillon et al. 2023; Zhang et al. 2023; Řezník et al. 2020) can be modeled and estimated.

Long-term satellite observations make it possible to track changes in LSP over recent decades and place them in the context of global change. Studies of global trends of LSP parameters, mainly SOS and EOS, based on MODIS and the Advanced Very High Resolution Radiometer (AVHRR) data showed variances across climatic regions over the Northen Hemisphere (Jeong et al. 2011; Zhang et al. 2014) and the worldwide (Zhang et al. 2014). While the first study points to significant shifts in SOS and EOS in Europe, the latter one finds the overall trends in Europe, and especially in its temperate climate region, generally insignificant. Yuan et al. (2024) provide an overview of the impacts of global climate change on agricultural production. Bartošová et al. (2025) present differences in long-term GP observations (1961–2021) from Czechia for wild plants and agricultural crops across three altitude intervals. They observed some asynchrony in phenological shifts, with agricultural crops showing more pronounced shifts towards the beginning of the season compared to wild plants especially in low (0–299 m) and mid altitudes (300–499 m).

The present study uses a Landsat time series spanning over 30 years (1986–2020) to investigate long-term trends in crop development and productivity across Czechia. Specifically, we focus on the following objectives:

1. Extracting selected crop phenological (start-of-season: SOS, end-of-season: EOS, length-of-season: LOS, and day of maximum-of-season: MAX_DOY) and productivity characteristics (namely the small and large integral of the seasonal curve, SINT and LINT, respectively).
2. Analysing crop-specific temporal patterns to understand how these phenological and productivity metrics evolve over time for different crop types.
3. Assessing the role of natural conditions by examining how the observed trends in crop development and productivity vary across agro-climatic regions of Czechia.

The innovative element lies in linking long-term satellite-derived crop metrics with regional agro-climatic variability, offering new insights into the spatial and temporal dynamics of agricultural systems under changing environmental conditions.

Based on GP observations (Bartošová et al. 2025), we formulate the following hypotheses:

H1: Significant temporal trends in LSP and productivity characteristics (SOS, EOS, LOS, MAX_DOY, SINT, LINT) are expected over the observed period (1986–2020).

H2: Variability in trends will be detectable across agro-climatic regions of Czechia, enabled by the use of high spatial resolution Landsat data and detailed knowledge of crop distribution.

The following crops (or groups of crops) were taken into account for the analysis 1) winter cereals (including winter wheat, winter barley, winter rye etc.), 2) spring cereals (including spring wheat, spring barley, oat, spring rye etc.), 3) winter rapeseed, 4) fodder crops (including alfalfa, clover etc.), 5) sugar beetroot and 6) corn. The reasons for this selection were following: 1) the selected crops are the most frequent ones in the conditions of Czechia as they represent ca. 93% of the arable land in the country, and 2) they represent crops with different requirements for growing conditions. For the purpose of the study, the definitions of the Vegetation Phenology and Productivity parameters by Copernicus Land Monitoring Service is used (HR-VPP: User Manual). The study builds on previous work of the authors when a radiative transfer model-based algorithm for retrieval of LAI from Sentinel-2 and Landsat data for dominant crop types in Czechia was proposed and implemented (Tomíček et al. 2021; Tomíček et al. 2022).

2. Study area

The area of interest covers the entire Czechia. We used the Czech national agroclimatic regionalization,

Tab. 1 Characteristics of climatic regions according to decree No. 327/1998 Coll. issued by the Ministry of Agriculture.

Region code	Region characteristic	Sum of temp. above 10 °C	Mean annual temp.	Mean annual precipitation
0:VT	very warm, dry	2800–3100	9–10 °C	500–600 mm
1:T1	warm, dry	2600–2800	8–9 °C	< 500 mm
2:T2	warm, mildly dry	2600–2800	8–9 °C	500–600 mm
3:T3	warm, mildly humid	2500–2800	(7)8–9 °C	550–650 (700) mm
4:MT1	mildly warm, dry	2400–2600	7–8.5 °C	450–550 mm
5:MT2	mildly warm, mildly humid	2200–2500	7–8 °C	550–650 (700) mm
6:MT3	mildly warm (to warm), humid	2500–2700	7.5–8.5 °C	700–900 mm
7:MT4	mildly warm, humid	2200–2400	6–7 °C	650–750 mm
8:MCh	mildly cold, humid	2000–2200	5–6 °C	700–800 mm
9:CH	cold, humid	< 2000	< 5 °C	> 800 mm

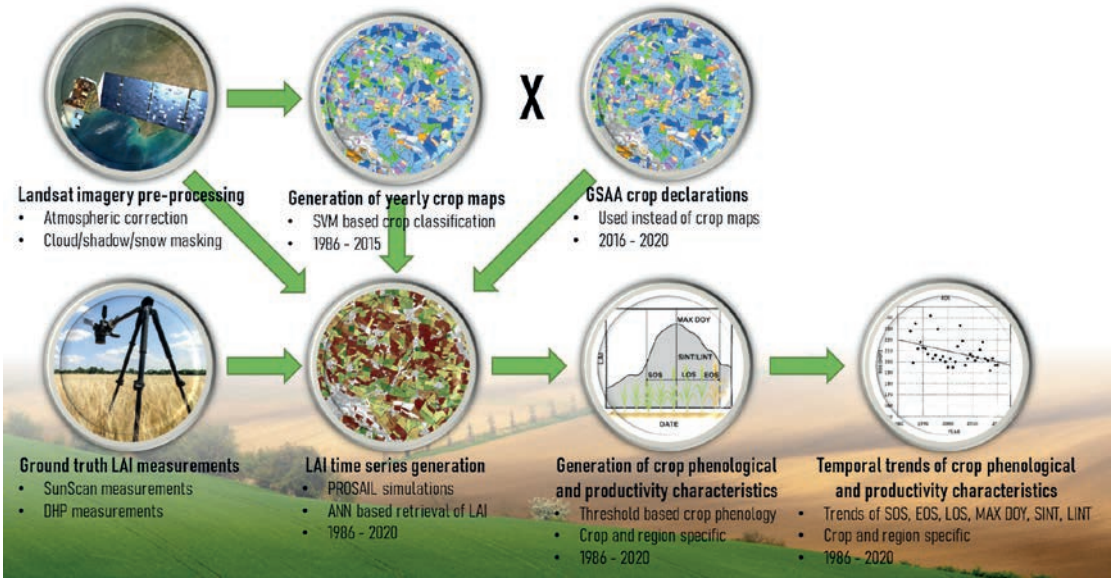

Fig. 1 Methodology and processing workflow comprising Landsat time series pre-processing, ground leaf area index (LAI) measurements, LAI retrieval based on the PROSAIL radiative transfer model and an artificial neural network (ANN) regression model, crop classification, derivation of crop phenological and productivity characteristics and their analysis over agroclimatic zones.

as defined by Decree No. 327/1998 Coll. issued by the Ministry of Agriculture (Decree No. 327/1998), which divides the territory of Czechia into 10 agroclimatic zones based on temperature and humidity characteristics. Table 1 contains the values of the key climatic characteristics of individual agroclimatic regions.

3. Materials and methods

The Landsat series of satellites has been providing high-resolution multispectral data for more than three decades. For the present study, the Landsat time series covered the period from 1986 to 2020. The overall methodology and processing workflow is depicted in Fig. 1 and described in detail in the following subsections 3.1–3.5.

3.1 Landsat imagery preprocessing

The Landsat spectral bands with native spatial resolution of 30 m were used in this study. The raw Level 1 scenes were processed to Level 2 (top-of-canopy reflectance) in the ARCSI (Atmospheric and Radiometric Correction of Satellite Imagery) software (ARCSI GitHub). Invalid or defective pixels (such as snow, cloud and shadows, saturated pixels, etc.) were masked using the FMask algorithm (Zhu and Woodcock 2012; Zhu et al. 2015).

3.2 Development of the Leaf Area Index retrieval model

3.2.1 Ground-truth LAI measurements

Ground-based LAI measurements were collected in Elbeland, a fertile lowland area in central Bohemia belonging to agroclimatic region T2 (average annual temperature 8–9 °C, precipitation 500–600 mm; Tab. 1). this area is considered one of the most fertile in the Czechia. Reference LAI values were measured using two methods: (1) with a Delta-T SunScan instrument (Webb et al. 2016), and (2) through digital hemispherical photography (DHP). At each sampling point (an area of approximately 20 × 20 m), either five SunScan measurements, eight DHP images, or both were collected – depending on site conditions – and averaged as reference values. Points where both DHP and SunScan LAI measurements were collected simultaneously allowed for direct comparison between the two methods. To maximize the consistency between the two LAI datasets, a simple linear transformation was applied to the SunScan-derived LAI values; see Tomíček et al. (2021) for more detailed description. In total, 432 points were measured on 39 plots in 2017 and 2018 in Elbeland, central Bohemia (Fig. 2). Reference data were used to calibrate and validate the LAI estimation model (section 3.2.2. for details). The campaigns were scheduled to cover key phenological phases of the growing season (campaign dates together with reference Landsat scenes are listed in Tab. 2).

3.2.2 LAI retrieval approach

The applied approach of LAI retrieval from high resolution satellite data was proposed in our previous studies (Tomíček et al. 2021; Tomíček et al. 2022). The developed algorithm uses crop-optimized PROSAIL radiative transfer model (RTM) to generate a database of simulations for training of the regression model. Ranges and distribution functions of biophysical, biochemical and structural parameters (the input parameters of the PROSAIL RTM) for individual crops of interest were derived based on an extensive dataset

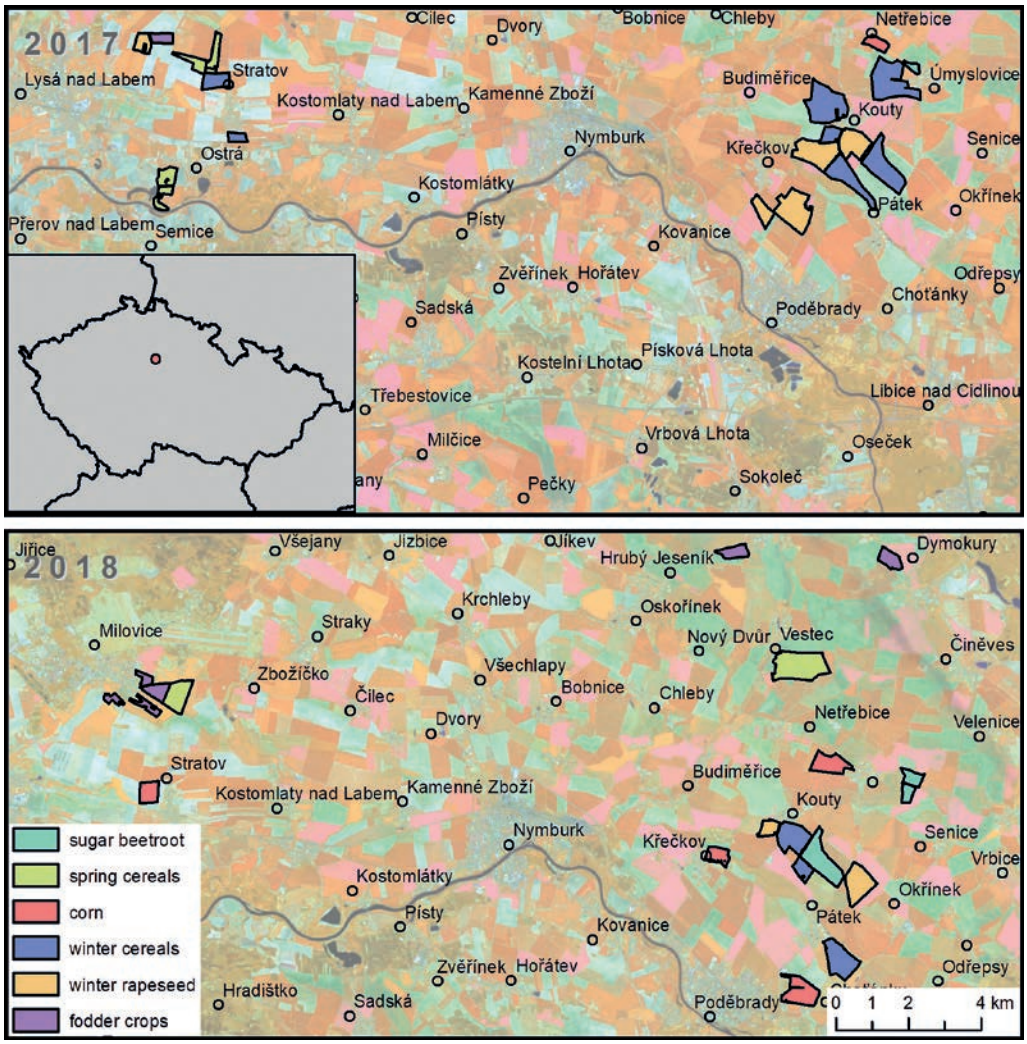

Fig. 2 Agricultural parcels where field campaigns took place in 2017 and 2018.

Tab. 2 Summary on field sampling dates and the reference Landsat scenes.

Date of field sampling	29.–31. 3. 2017	17.–19. 5. 2017	19.–21. 6. 2017	27.–30. 4. 2018	21. 5. 2018	26. 7. 2018
Reference Landsat scene	1. 4. 2017	19. 5. 2017	20. 6. 2017	28. 4. 2018	22. 5. 2018	25. 7. 2018

of field measurements and an empirical parametrization procedure (Tomíček et al. 2021).

We used an artificial neural network (ANN) approach as the regression model for LAI quantitative estimation. Despite its "black-box" nature, this approach provides the ability to implicitly model complex nonlinear relationships between model inputs and outputs (Richter et al. 2012). Using the TensorFlow python library, a feed-forward neural network with one hidden layer was implemented, the widely used rectified linear unit (ReLu) was chosen as the activation function (Wolanin et al. 2019; Xu et al. 2022). To evaluate model performance, the training dataset were divided into calibration (80%) and validation (20%) subsets, and mean squared error was tracked as the loss function within an early stopping mechanism (Tomíček et al. 2021).

The accuracy assessment was performed on cloud-free images with a maximum time delay of 5 days from the collection of ground-truth reference data. For most crops of interest, RMSE was below 1 (except for spring cereals, RMSE = 1.36 and winter rapeseed, RMSE = 2.38) and R^2 was above or equal to 0.7 (except for spring cereals, R^2 = 0.48), Tomíček et al. (2022) for detailed validation results.

3.3 Generation of yearly crop maps

Since changes in phenological and productivity characteristics are monitored specifically for different crops, it was first necessary to know spatial pattern of the crops for the considered growing seasons. Unfortunately, a systematic registry of crop type cultivated on particular agricultural parcels is available only

from 2016 onwards; LPIS/GSAA registry data was provided by the State Agricultural Intervention Fund. Therefore, the spatial patterns of the considered crops for the period before 2016 had to be obtained by an alternative way – in this case by supervised classification of Landsat satellite data.

Multitemporal composites were generated first from the source imagery using quarterly time step. The main aim of such temporal aggregation was to cover the entire area of interest by valid data for the given period with no (or at least minimum) occurrence of "nodata gaps" caused by clouds, shadows or snow. The aggregation was based on calculating weighted average of the input reflectance values taking into account 1) spatial distance of the given pixel to the nearest cloud/shadow/snow (the further the pixel is, the higher weight it gets) and 2) temporal distance of the given data acquisition to the mid-date of the used compositing period (scenes acquired closer to the mid-date are preferred over those acquired at the beginning or the end of the period).

Support Vector Machine (SVM) classifier was used for classification of the crop classes: 1) winter cereals, 2) spring cereals, 3) winter rapeseed, 4) fodder crops, 5) sugar beetroot, 6) corn and 7) other crops. The two input parameters of the SVM classifier (C and gamma) were automatically tuned by repeated training to find the best performing configuration. Also, two different kernels (linear and RBF) of the algorithm were considered. The described crop classification was applied under a cropland mask derived from (a) archival LPIS data (available from 2004 onwards) and (b) an internal land cover classification, which accounts for cropland areas not included in the 2004 LPIS dataset. The crop classification procedure then resulted in a thematic raster layer (crop map) and a pixel-based probability layer. The last step was postprocessing, including thematic filtering (pixels with a probability below 70% were reassigned to the "other crops" class) and spatial filtering using a sieve filter (the minimum mapping unit was set at 10 pixels).

Reference data used for training the SVM classifier as well as for validation of the output crop classification maps were obtained by visual interpretation of Landsat images. The visual interpretation was performed using false-colour RGB combination of NIR, SWIR-1 and SWIR-2 bands, which was found to be the most suitable spectral combination for identification of the different crop types. Plots for this visual interpretation were selected randomly across the entire Czechia, with particular attention given to cases where there was high certainty regarding the assigned/interpreted crop type. In addition, independent validation dataset was created as well. However, as the visual interpretation of crop types was highly time demanding, validation data were interpreted only for some years (1986, 1993, 2000, 2002, 2011, 2012). Selection of the reference years took into account two different aspect: 1) quality of the input imagery used for visual interpretation and 2) main phases of the economic development of Czechia (1986: late phase of the socialistic regime, 1993: beginning of economic transformation, restitutions and privatization of agricultural land, 2000 and 2002: preparation for the EU membership, 2011, 2012: EU membership). For each validation year, between 400 and 500 parcels were analysed.

3.4 LAI time series generation

Successful determination of phenological and productivity parameters from remote sensing imagery requires a relatively dense time series of observations. However, for the vast majority of the period of interest

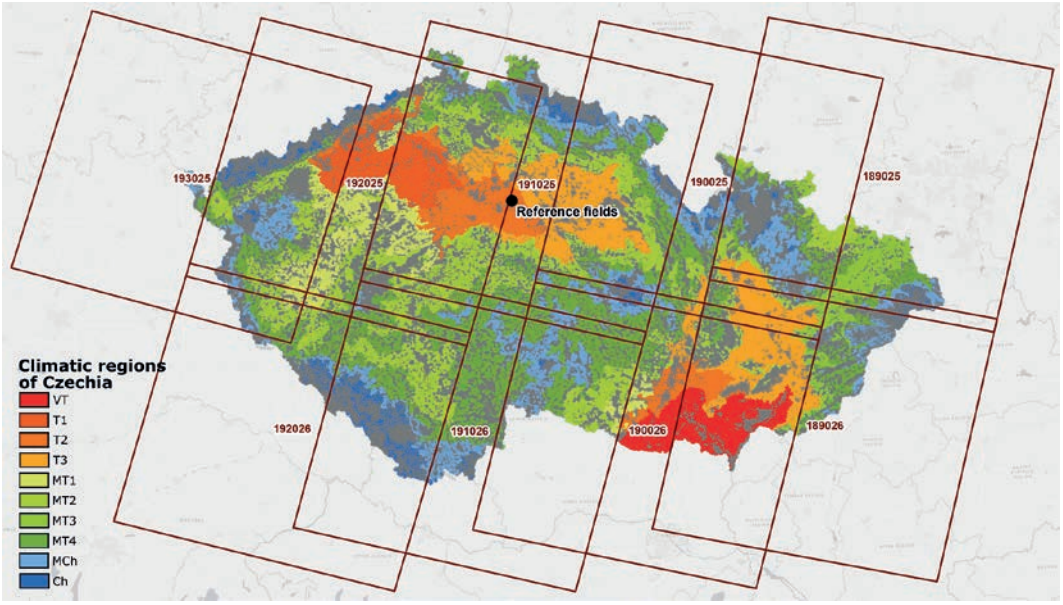

Fig. 3 Landsat tiles covering the territory of Czechia together with agroclimatic regions.

between 1986 and 2020, only Landsat data are available, with a revisit time of 16 days. To overcome this problem, Landsat-derived LAI products were spatially aggregated based on agroclimatic regions (described in section 2), where each of the regions spans two or more Landsat tiles (Fig. 3). The key assumption was that climatic conditions play a fundamental role in the timing of the phenological cycle of vegetation.

Zonal median of LAI was calculated for each single acquisition date of the source imagery and for all existing combination of agroclimatic region and crop. The number of dates for which aggregated LAI values are available is then considerably higher compared to the situation when LAI is considered locally (e.g. on parcel or point level).

3.5 Determination of crop phenological and productivity characteristics

Annual time series of the LAI values were filtered by the Savitzky-Golay filter as a first step to suppress influence of noise in the source data. In the next step, a radial basis function (RBF) was fitted to interpolate the LAI seasonal profile within a 1-day step. A 'threshold approach' was then applied to extract phenological (SOS, EOS, LOS, MAX_DOY) and productivity (SINT, LINT) parameters. The threshold approach uses a certain percentage of the annual LAI amplitude (i.e., the difference between the annual maximum and minimum LAI) as a threshold to determine the timing of phenological phases.

In the case of our study, 25% of the LAI annual amplitude was set as the threshold value. Date, when LAI first reaches such threshold is then considered as the SOS date, whereas EOS date is then considered as the day when LAI drops below the threshold. The date of reaching the annual LAI maximum is MAX_DOY, the period between SOS and EOS is then considered as LOS. Smoothed and interpolated LAI profiles were also used for extraction of vegetation productivity indicators (small integral, SINT and large integral, LINT). Both of these indicators represent area under the LAI temporal curve. The difference is that the LINT takes into account full area under curve (i.e. above LAI = 0), whereas the SINT indicator takes into account only the area under curve above the baseline defined as the annual LAI minimum. The principle of determining phenological and productivity parameters is shown in the diagram in Fig. 4. The described approach is used for example in case of TIMESAT software (Eklundh and Jönsson 2015) which is applied for production of the High Resolution Vegetation Phenology and Productivity (HR-VPP) products under the Copernicus Land Monitoring Service (CLMS). The SINT and LINT indicators show a strong correlation specifically with the SPROD (seasonal productivity) and TPROD (total productivity) parameters produced in the HR-VPP dataset.

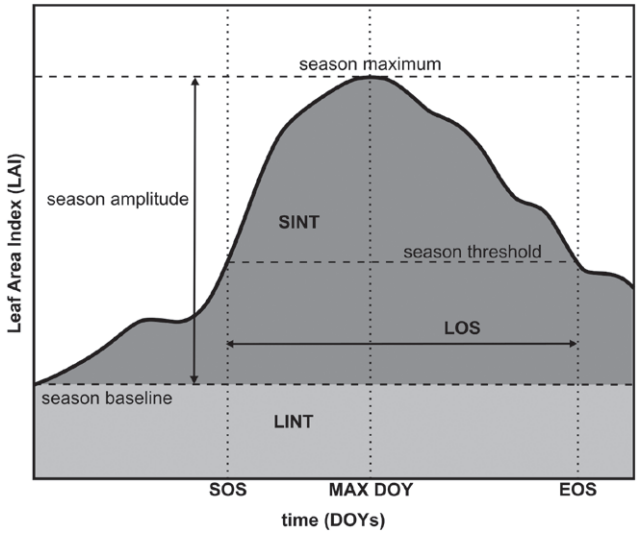

Fig. 4 Diagram illustrating the principle used to determine phenological and productivity parameters.

The 35-year evolution of phenological and productivity parameters was then examined using linear least squares regression. For each combination of a) climatic region, b) crop and c) phenological or productivity parameter, the slope of the regression line was calculated. The statistical significance of the trend was verified using the Wald test with the t-distribution of the test statistic. The Wald statistic results from dividing the regression coefficient by its corresponding standard error; the null hypothesis states that the slope is equal to zero.

In order to compare the influence of the agroclimatic regions, the differences in slope values between regions were calculated for each LSP, productivity parameter and crop individually. To ensure consistency in the sign of the differences, the slope value corresponding to the colder agroclimatic region was always subtracted from that corresponding to the warmer region. A Wilcoxon signed-rank test was used to test the null hypothesis that the median of differences in slope values equals zero for six crops and six parameters (36 cases in total). Rejecting the null hypothesis indicated a systematic shift in the slope of the given combination of parameters and crops across the agroclimatic regions.

4. Results

4.1 Crop classification accuracy assessment

Two raster layers (thematic crop map and probability map) were obtained for each year of the 1986–2015 period as the output of the SVM classification model. These layers were further the subject of quality assessment based on a standardized validation workflow calculating class-related accuracy indicators (user's and producer's accuracy and F-1 score) as

well as the overall accuracy. For all validation years, the overall accuracy was higher than 80%. We expect similar accuracy characteristics for the rest of the years since the same crop classification workflow was applied there. The results of the crop classification accuracy assessment are shown in Tab. 3.

4.2 Aggregated LAI time series

The set of six plots in Fig. 5 shows examples of seasonal time series for six crops of interest: 1) winter cereals, 2) spring cereals, 3) winter rapeseed, 4) fodder crops, 5) sugar beetroot and 6) corn derived by spatial aggregation of the original LAI layers within the extent of agro-climatic regions (data for the year 2018 and agro-climatic region MT1 were used here). The original LAI values derived from the spectral information of the Landsat data (hollow circles) were smoothed using the Savitzky-golay filter (solid black dots) and, as a final step, interpolated with a 1-day step using the RBF function (black line). The quality of the created seasonal LAI time series is crucial for the correct determination of the phenological and productivity characteristics of the stand.

4.3 35-year development of phenology and productivity

Fig. 6 shows an example of the 35-year evolution of the six phenological and productivity parameters of interest (SOS, EOS, LOS, MAX_DOY, SINT and LINT) for winter cereals and climate region VT. Values for individual years were fitted with a regression line determined by the method of least squares for trend evaluation. The p-value determines the significance of the observed trend (in this case, the trend is significant for parameters EOS and MAX_DOY).

The magnitude of the trend (slope of the regression line) of the 35-year evolution of the phenological and productivity parameters of interest is visualized in Fig. 7. The exact values together with their significance are then summarized in Appendix 1. Only a few significant trends were documented in the case of the phenological parameters SOS and LOS. Moreover, the variability of slope values was relatively high across crops and climatic regions. However, a significant negative trend occurred in the case of EOS and MAX-DOY phenological parameters in most climatic regions of crops: winter cereals, spring cereals, winter rapeseed and fodder crops, i.e. all crops with the exception of the so-called summer crops (sugar beetroot and corn). Specifically, for EOS, a significant trend was demonstrated for winter cereals in 10, spring cereals in 7, winter rapeseed in 8 and fodder crops in 7 climate regions out of 10; for MAX-DOY there were 10 occurrences for winter cereals, 8 for spring cereals, 7 for winter rapeseed and 6 for fodder crops. The slope of the regression line (the magnitude of the trend) for the parameter MAX-DOY was in the range of −0.4 and −0.7 in 90% of significant cases. In

Tab. 3 Crop classification accuracy assessment metrics (W.C. = winter cereals, S.C. = spring cereals, W.R. = winter rapeseed, F.C. = fodder crops, S.B. = sugar beetroot, C. = corn, OA = overall accuracy, UA = user's accuracy, PA = producer's accuracy, F1 = F-1 score).

Parameter		W.C.	S.C.	W.R.	F.C.	S.B.	C.	OA
1986	UA	86.6	40.7	96.0	92.5	93.4	78.5	80.1 (n = 433)
	PA	56.9	68.6	95.1	86.0	91.9	86.4	
	F1	68.6	51.1	95.6	89.1	92.7	82.3	
1993	UA	96.2	92.3	100.0	100.0	75.9	97.2	93.3 (n = 434)
	PA	100.0	96.0	98.1	100.0	96.9	60.3	
	F1	98.0	94.1	99.0	100.0	85.1	74.5	
2000	UA	100.0	77.3	100.0	100.0	96.4	94.8	95.3 (n = 424)
	PA	91.0	98.1	97.1	93.0	96.4	98.2	
	F1	95.3	86.4	98.5	96.4	96.4	96.5	
2002	UA	96.7	72.9	97.4	100.0	87.8	94.1	92.2 (n = 503)
	PA	87.3	94.4	99.1	93.8	93.5	84.2	
	F1	91.8	82.3	98.2	96.8	90.6	88.9	
2011	UA	93.3	73.8	100.0	100.0	98.2	100.0	94.4 (n = 430)
	PA	95.1	86.5	97.1	100.0	100.0	85.5	
	F1	94.2	79.6	98.5	100.0	99.1	92.2	
2012	UA	75.4	96.7	96.7	97.5	97.4	69.7	85.4 (n = 397)
	PA	98.0	56.9	89.0	92.9	67.9	95.8	
	F1	85.2	71.6	92.7	95.1	80.0	80.7	

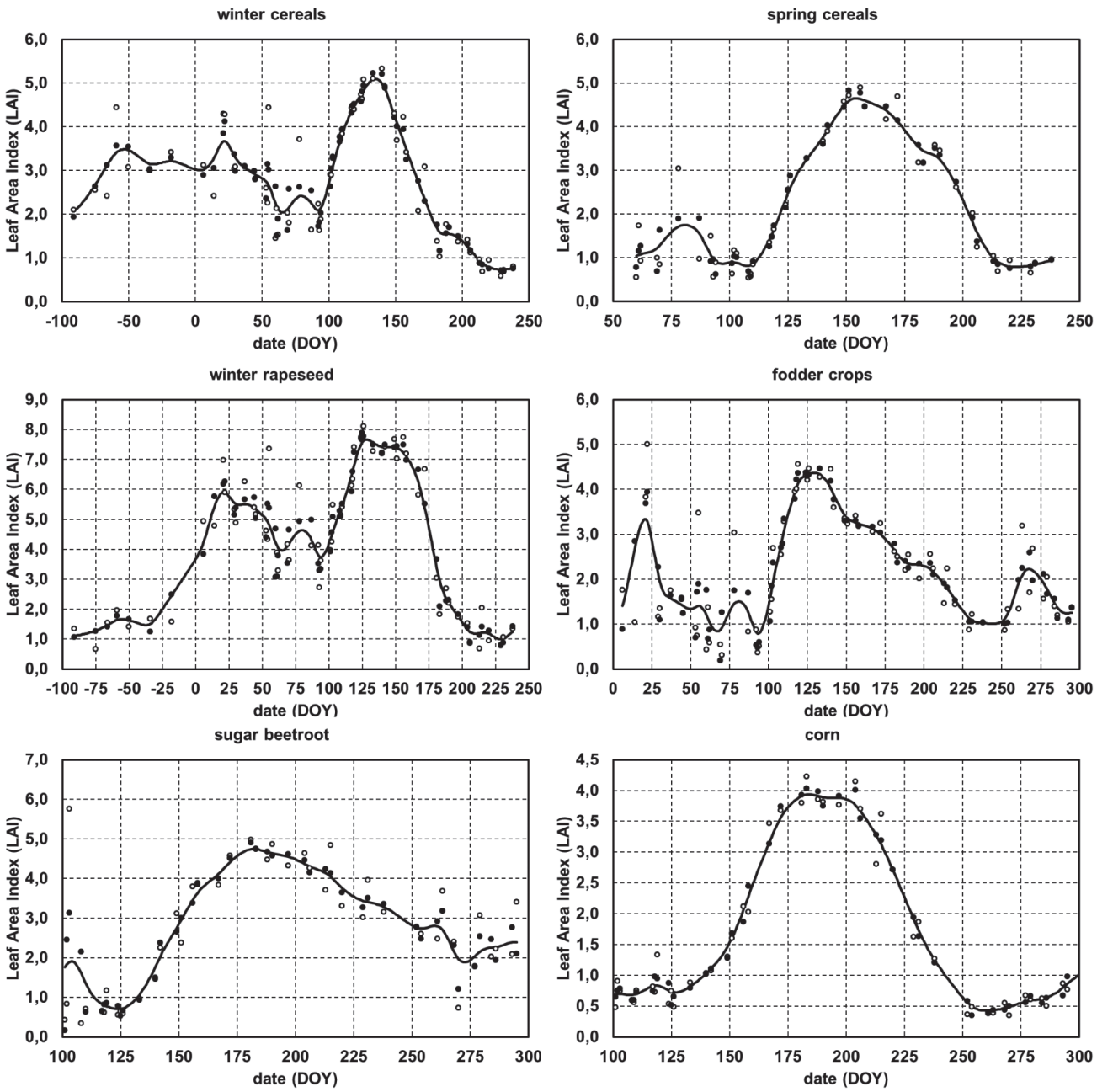

Fig. 5 Example of the aggregated LAI time series for six crops of interest. The original retrieval value is shown by the hollow circles, the solid black dots represent the filtered values, and the values interpolated by the RBF function to a 1-day step are symbolized by the black line.

contrast, slope values varied more between crops in the EOS case. While for winter cereals, spring cereals and winter rapeseed, the slope was between −0.3 and −0.5 in 92% of significant cases, for the fodder crops the slope was between −0.7 and −1.6 in all significant cases.

In the case of productivity parameters, a significant trend in more than half of the climate regions occurred only for spring cereals and sugar beetroot SINT (8 and 6 occurrences out of 10, respectively).

Fig. 8 shows boxplots depicting the mean and dispersion statistics of the differences in LSP and productivity parameter slope values between agroclimatic regions for each crop. The null hypothesis revealed that the median difference was significant in 15 out of 36 cases: six of these were positive and nine were negative. In the majority of cases, the slope values themselves were consistently either positive or negative for a given crop type and observed parameter (Fig. 7 and Appendix 1). Therefore, a positive median difference indicates that the slope value decreases when moving from warmer to colder regions. This implies that shifts in the LSP and productivity parameters were more pronounced in warmer regions during the observed period, provided the slope values were both positive. Conversely, when both slopes were negative, stronger shifts in the observed parameters occurred in the colder regions.

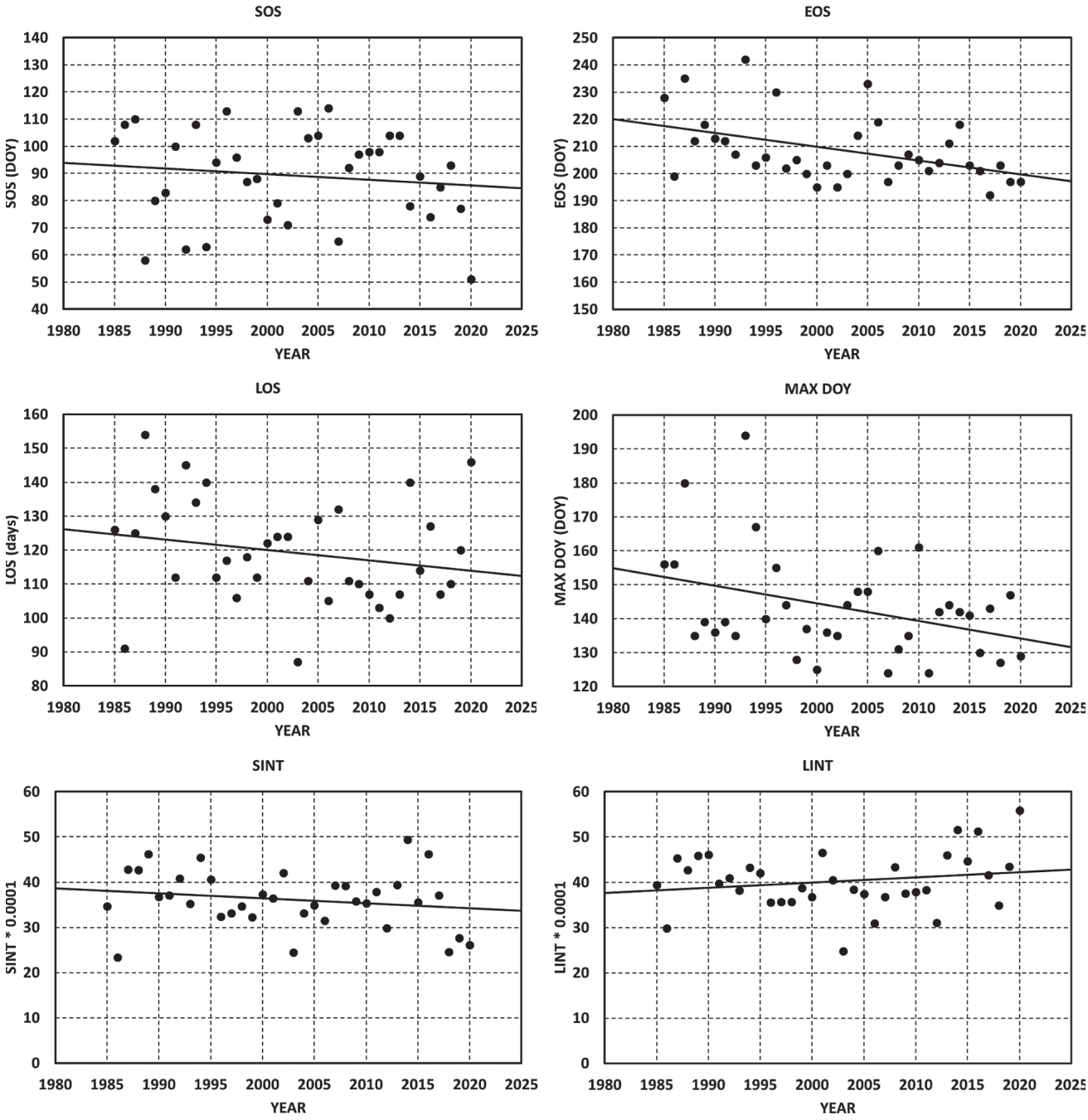

Fig. 6 Example for the 35-year evolution of SOS, EOS, LOS, MAX-DOY, SINT a LINT for winter cereals and climate region VT.

5. Discussion

5.1 Retrieval of LSP parameters

Different vegetation spectral indices such as NDVI or EVI are used for LSP due to their ease of calculation (Misra et al. 2020; Zhang et al. 2023). In accordance with (Lu et al. 2025), the choice of LAI can be supported by its biophysical relevance. By measuring the total leaf area per unit ground area, LAI directly reflects vegetation structure and function. It is closely linked to photosynthesis, transpiration, and carbon fluxes, making it a more meaningful physiological indicator than purely spectral indices. Moreover, LAI is more sensitive than NDVI to canopy development and senescence, particularly in areas with high vegetation. It provides a quantitative measure of vegetation growth stages, which is crucial for modeling ecosystem processes. Furthermore, significant progress has been made in recent years in retrieving LAI based on machine learning and radiative transfer models (Tomíček at al. 2021; Qin et al. 2024).

The accuracy of derived LAI with RMSE = 1.36 for spring cereals, RMSE = 2.38 for winter rapeseed, and RMSE < 1 for other crops (Tomíček et al. 2022) is comparable with other models. (Mourad et al. 2020)

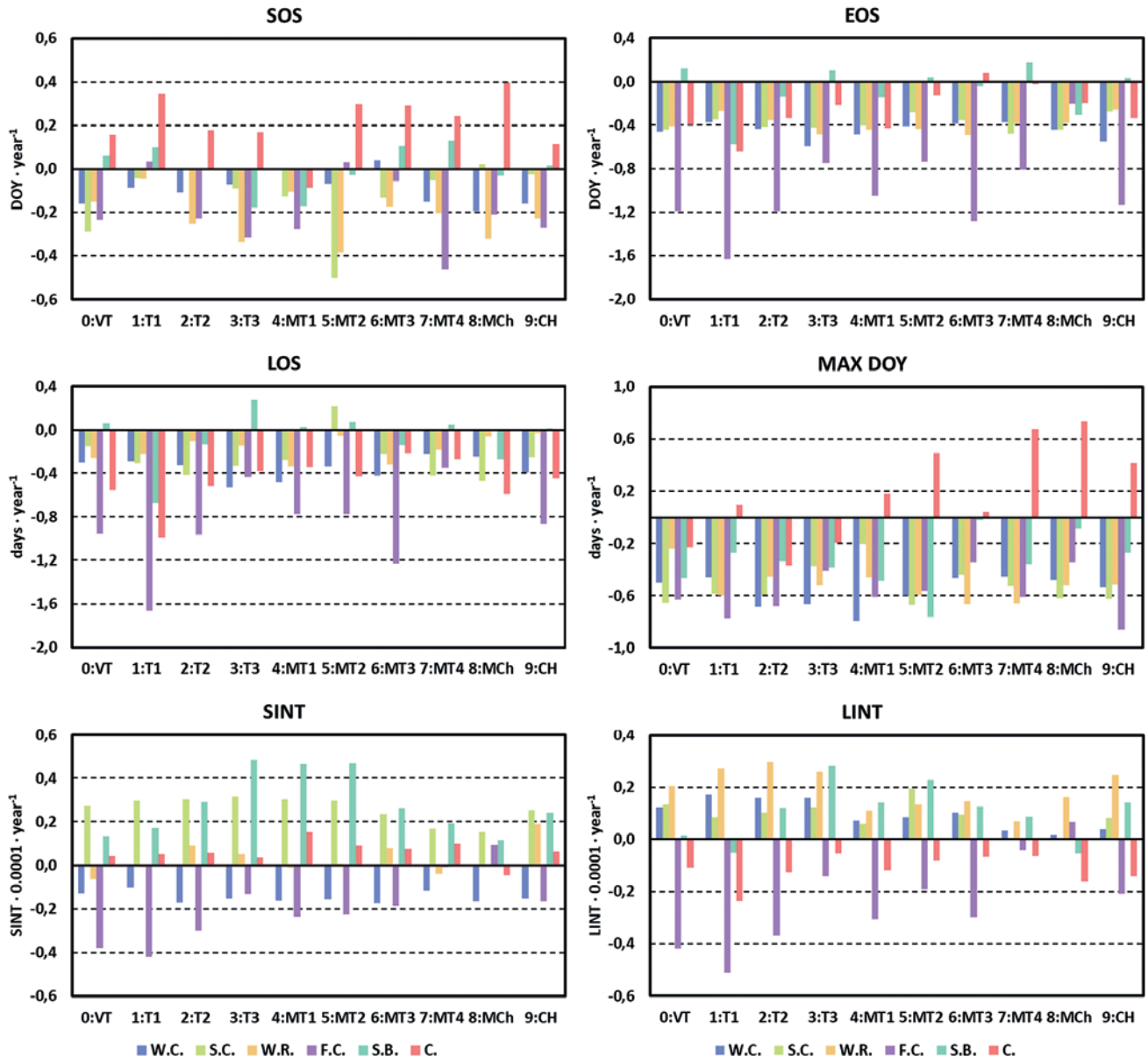

Fig. 7 Slope of individual phenological and productivity parameters derived over all combinations of climatic regions and crops (W.C. = winter cereals, S.C. = spring cereals, W.R. = winter rapeseed, F.C. = fodder crops, S.B. = sugar beetroot, C. = corn).

evaluated empirical models for LAI derivation from NDVI, EVI2, and soil adjusted vegetation index (SAVI) as well as a biophysical model based on ANN embedded to the ESA Sentinel Application Platform (SNAP) software applied on Snetinel-2 and HLS product. After comparison to in-situ measurement, the best models revealed RMSE between 0.65 and 0.89 for corns (barley and wheat). Similarly to our approach, Dhakar et al. (2021) conducted retrieval of wheat LAI by LUT-based inversion of PROSAIL-5B model using atmospherically corrected Landsat-8 OLI reflectance. They achieved a good agreement with the in-situ observed LAI having RMSE of 0.70.

Two main methods are often used to determine Land Surface Phenology (LPS) metrics from satellite data: the threshold method (used for example in Timesat tool; Jönsson and Eklundh 2004) and the derivative method (used for example in HANTS workflow; Zhou et al. 2015). The threshold method determines phenological events (such as SOS or EOS) based on crossing a fixed level of the used variable (e.g. LAI) typically corresponding to a certain percentage of its seasonal maximum or seasonal amplitude. The threshold method is simple, intuitive and easy to implement. It is also more tolerant to presence of moderate noise in the input data if the thresholds are chosen properly. Another advantage can be also seen in its flexibility since the thresholds can be adjusted independently for different types of vegetation. On the contrary, the biggest disadvantages of this method include primarily its sensitivity to the threshold choice when there is generally no exact clue on what percentage of the season maximum (or amplitude) is appropriate to be considered as start/end of

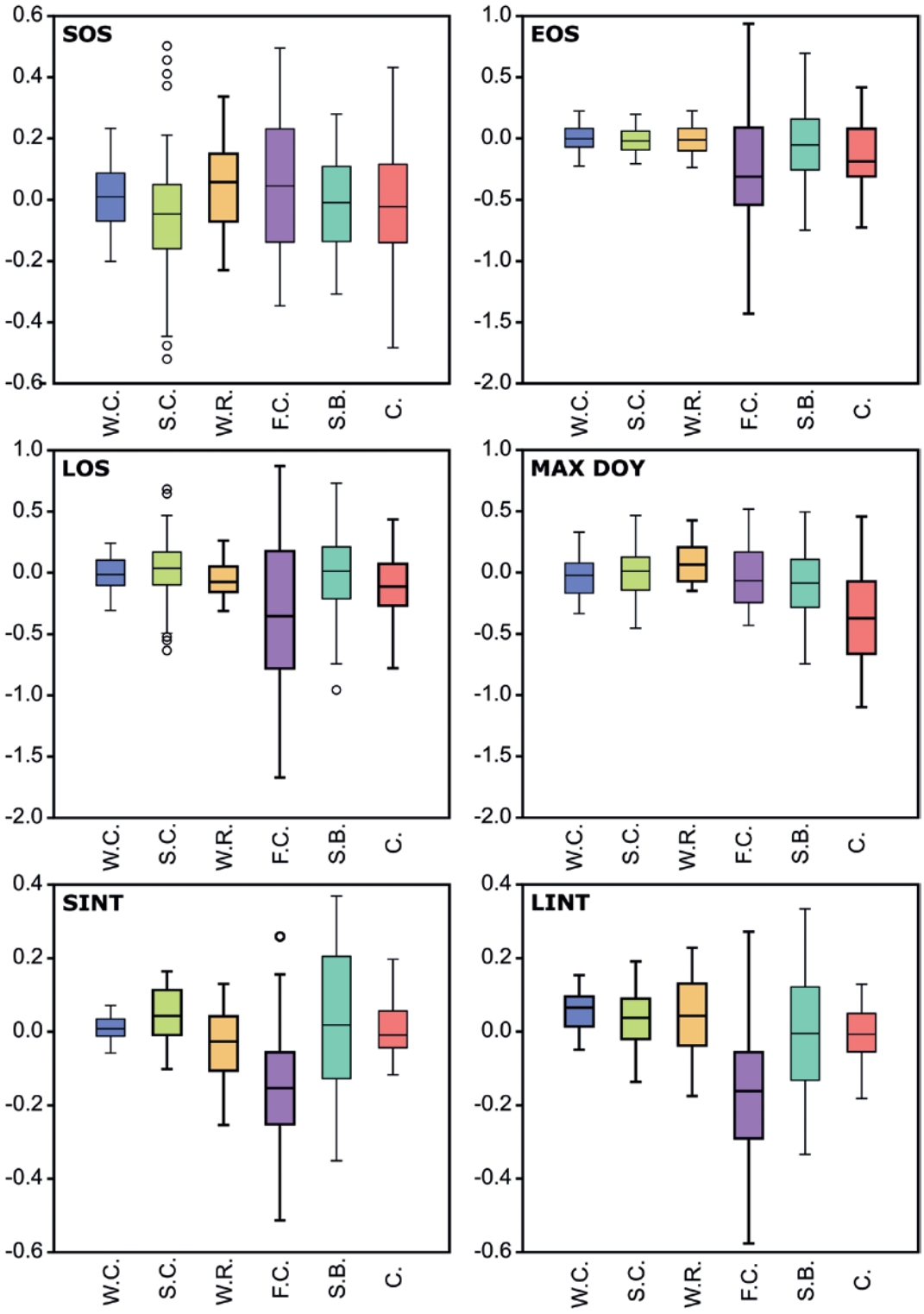

Fig. 8 Statistics of differences in LSP and productivity parameters slope values between agroclimatic regions calculated for each crop. Significant cases are highlighted in bold.

the season (e.g. Huang et al. 2019). In addition, the threshold method is not very suitable for such case typical for flat phenological profiles (i.e. low seasonal amplitudes). It may also miss the full shape and complexity of the phenological curve (this happen especially in cases where multiple growing season are present at the given place). In summary, the threshold method seems to be ideal for rapid applications or in cases when lower-quality of the data is expected on the input. The derivative method identifies phenological events based on the rate of change in the input variable (e.g. LAI) typically by finding the inflection points using first derivative. Thus, there is no need to define any thresholds and the condition for detection

of the main phenological events (such as SOS and EOS) are there clearly defined. It is also better capturing full dynamics of the phenological profile and thus it is more suitable in in cases typical for rapid LAI transitions (i.e. as a spring "green-up"). On the other hand, performance of the derivative method is highly sensitive to noise in the input data and thus needs high quality and well-smoothed inputs (e.g. de Beurs and Henebry 2009). From implementation perspective, it is more complex (taking into account all the fitting and smoothing steps before applying derivative) and maybe less intuitive compared to the threshold method.

5.2 Crop types classification and its accuracy

Knowledge of crop types and their spatial distribution was a crucial to the present study. As the information from the LPIS/GSAA registry was unavailable before 2016, supervised classification based on quarterly cloud free mosaics of Landsat imagery was carried out instead. A comparative study performed by (Pluto-Kossakowska 2021) showed that there are no significant differences in accuracy when utilizing different machine learning (ML) algorithms for the multitemporal classification of satellite images for crop and arable land recognition. According to their findings, the ANN classifiers perform just a few percent better than ML. Among ML algorithms, SVM and Random Forest (RF) are commonly used. User's accuracy achieved by our approach based on SVM algorithm is comparable to or outperforms the results collected by (Pluto-Kossakowska 2021) as shown in Tab. 4. (Van Tricht et al. 2023) developed an open-source system for global-scale, seasonal, and reproducible crop and irrigation mapping. Their classification approach is based on decision trees and Landsat and Sentinel-2 imagery. They claim user's (and producer's) accuracy of 94 and 86 (78 and 76)% for cereals and corn, respectively. (Huang et al. 2022) focused on winter cereals in Europe between 2016 and 2020. They combined Landsat and Sentinel-2 imagery with Sentinel-1 SAR data in order to discriminate between winter cereals and winter rapeseed. They implemented a time-weighted dynamic time warping (TWDTW) method, based on the comparison of seasonal changes in NDVI with standard seasonal changes, as well as RF classification, achieving overall accuracies of 91 and 81%, respectively. Specifically, in Czechia, they reached equal user's and producer's accuracies of 87% in discriminating winter cereals. Thus, the classification accuracy based on the SVM algorithm as applied in our study is among the best achieved using comparable methods on Landsat imagery.

5.3 Phenological and productivity trends and their relation to the crop types and climate regions

5.3.1 General trends of LSP and productivity parameters

Over the last 40 years, LSP has undergone changes that vary by climate region and fluctuate over time. Jeong et al. (2011) observed an increase in LOS of temperate vegetation in the Northern Hemisphere between 1982 and 2008. They based their results on analyzing NDVI derived from AVHRR and temperatures. However, the SOS advance of 5.2 and 0.2 days and the EOS delay of 4.3 and 2.3 days differed between the 1982–1999 and 2000–2008 periods, respectively. Specifically in Europe, the delayed EOS of 8.2 days was more significant than the advanced SOS of 3.2 days in the latter period. Global LSP based on AVHRR and MODIS data from 1982 to 2010 was also studied by (Zhang et al. 2014). The seasonal vegetative trajectory was derived from daily EVI across Köppen's climate regions. The analysis showed that SOS generally shifted early in temperate, cold and polar climates in the Northern Hemisphere. However, areas with a significantly earlier SOS decreased in number between 2000 and 2010 compared to the period between 1982 and 1999, and LOS also increased. Notably, the overall trends in Europe were generally insignificant.

In our study, we calculated and analyzed trends in the six LSP and productivity characteristics of six crops over ten agroclimatic regions of Czechia between 1986 and 2020. Overall, there was no significant trend of SOS for the studied agricultural crops except for winter rapeseed in regions T3 and MCh. Nevertheless, there was a general trend towards earlier SOS for most crops except for sugar beetroot and corn. On average, the shift was 1.1 day per decade for winter and spring cereals, and 2.1 day for winter rapeseed and fodder crops. Similar SOS behavior of rainfed and irrigated crops was observed in Spain (Michavila et al. 2024). The later occurrence of SOS of corn, which has a later emergence, is in accordance with study carried out the Midwest of the United States (Zhang et al. 2019). The EOS trend was significant in a greater number of crops and agroclimatic regions, with an average shift of 5.6 days per decade for the four most significant crops. Contrary to the findings of (Jeong et al. 2011) but in accordance with those of (Michavila et

Tab. 4 Average user's accuracy (UA) achieved by SVM classification of Landsat images compared to accuracies reported for the same crops by (Pluto-Kossakowska, 2021). In the case of rapeseed and sugar beetroot only RF classification results were available in the reference literature.

	Winter cereals	Spring cereals	Rapeseed	Sugar beetroot	Corn
UA our study %	91	76	98	92	89
UA P-K %	72	53	96	79	90

al. 2024), this shift is negative, i.e. towards an earlier DOY. It should be noted that both Jeong et al. (2011) and Zhang et al. (2014) focused on vegetation in general. The LSP parameters of agricultural crops are specific because, in addition to natural processes such as temperature, day length or precipitation, they are also determined by human management decisions such as the actual planting and harvest days, irrigation, fertilization and pests and weed control (Bartošová et al. 2025). Moreover, in the case of agricultural crops, the EOS does not represent the biological termination of the vegetation curve, as it does for natural vegetation. Instead, the senescence phase of the curve is artificially shortened by harvesting, with the harvest date primarily depending on the timing of crop maturity. Therefore, they are not fully comparable. Even when only agricultural plots are considered, the coarser resolution of MODIS or AVHRR causes slight changes to SOS and EOS trends due to the surrounding natural vegetation mixing with crops in the fragmented agricultural landscape (Sisheber et al. 2023).

In general, the significance of the LOS trend was low in our study. On average, it tended towards a shortening of 3.5 days per decade which is again contrary to the findings of Jeong et al. (2011). The shortening of LOS is mainly caused by the advance of EOS. The LAI maximum (MAX_DOY) trends show similar patterns of significance to those of EOS (Appendix 1). Also, its average advance of 5.5 days per decade for the four most significant crops is almost equal to the shift in EOS. On the other hand, the negative trends of the four LSP parameters discussed are in accordance with predictions of changes in the time of sowing, flowering and maturity of cereals in Europe due to climate change (Olesen et al. 2012)but also affected by day length and potential physiological stresses. Responses may vary between species and varieties. Climate change will affect the timing of cereal crop development, but exact changes will also depend on changes in varieties as affected by plant breeding and variety choices. This study aimed to assess changes in timing of major phenological stages of cereal crops in Northern and Central Europe under climate change. Records on dates of sowing, flowering, and maturity of wheat, oats and maize were collected from field experiments conducted during the period 1985–2009. Data for spring wheat and spring oats covered latitudes from 46 to 64°N, winter wheat from 46 to 61°N, and maize from 47 to 58°N. The number of observations (site-year-variety combinations, given an average temperature increase of 0.35°C per decade in Czechia (Crhová et al. 2022.

Examining crop types, most significant trends in LSP parameters relate to winter and spring cereals, winter rapeseed, and fodder crops. All these crops show a trend of EOS and MAX_DOY advancement but they do not differ considerably across the agroclimatic regions except for fodder crops that exhibit the most pronounced trend, as well as greatest variability in EOS (Fig. 7). Fodder crops are harvested at least twice during the season (Springer and Aiken, 2015)theoretical ethanol yield, crude protein (CP. The timing and frequency are determined by natural conditions, such as soil type, temperature and precipitation. However, they mainly depend on whether the crop is harvested for forage or seed. Thus, increasing temperatures might explain the advance in harvest and different management practices the higher variability.

The productivity parameters vary in terms of their signs and values. A significant increase in the SINT can be observed for spring cereals and for sugar beetroot in 9 and 6 of the agroclimatic regions, respectively. An opposite trend, though significant only in two warmest regions, is evident for fodder crops and winter cereals (with no significant cases). For the LINT parameter, significant trends appear mostly for non-cereals in warmer regions. Again, LINT trends are not significant for winter cereals, but they have an opposite sign, which can be interpreted as an increase in total LAI while the area above the seasonal baseline was decreasing (Fig. 4).

5.3.2 Relation of LSP and production parameters to agroclimatic regions

Evaluating the differences in the slopes of the LSP parameters between the agroclimatic regions revealed a significant dependence in one-third of the 24 cases (i.e. four parameters times six crops), but this did not apply to cereals. The significant positive median slope differences in SOS and MAX_DOY for winter rapeseed indicate that the advance of SOS and MAX_DOY was higher in the colder regions, of around 0.5 days per decade for both parameters. The other significant shifts (fodder crops – EOS and LOS; corn – EOS, LOS, and MAX_DOY; and winter rapeseed – LOS) exhibited negative median differences. These observations suggest that during the observed period, the advancement of the harvesting of fodder crops and corn and the shortening of the production season were larger in warmer regions than in colder ones. When interpreting the negative median difference in the MAX_DOY parameter for corn, the sign of the slope must be considered. While it shows slight advancement in warmer regions, there is a trend towards later DOY in colder regions. This is consistent with the idea of using colder regions to grow crops that were previously only suitable for warmer regions, as discussed in relation to northern Europe, for example (Unc et al. 2021).

Bartošová et al. (2025) examined the relationship between elevation and the phenological phases of winter wheat. They analyzed in-situ observations of registered winter wheat cultivars at 17 experimental stations in Czechia between 1961 and 2021. The three stages evaluated were: i) jointing (first node at least 1 cm above the node); ii) heading (beginning of heading); and iii) ripening (fully ripe, hardened grains). The observations were grouped into

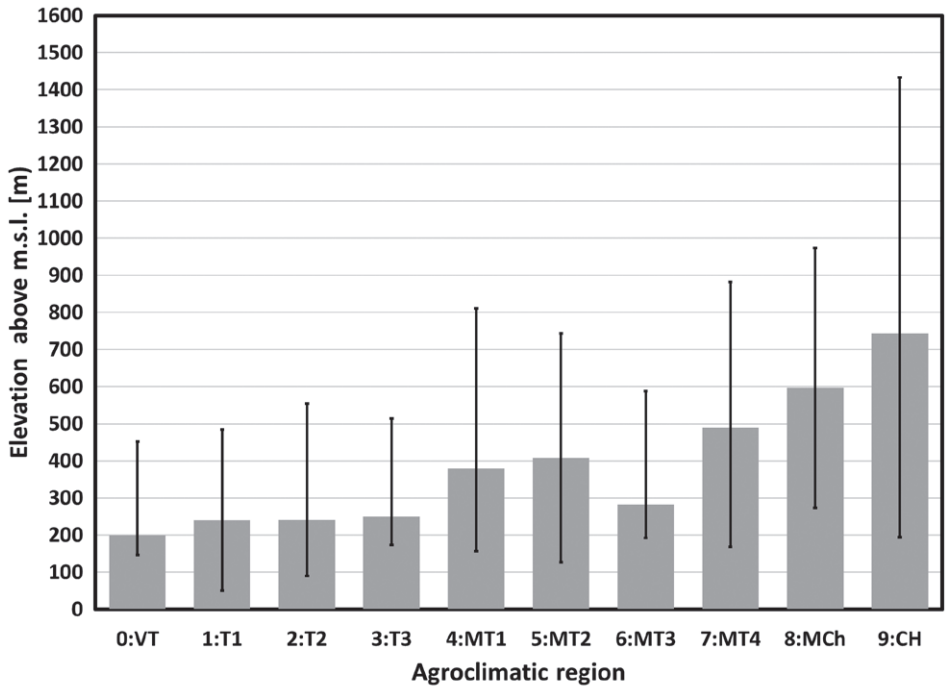

Fig. 9 Median, minimum, and maximum elevation calculated within the agroclimatic regions.

three elevation categories: 0–299 m, 300–499 m, and 500–750 m above mean sea level (a.m.s.l.). The agroclimatic regions used in our study cover a variety of elevations, as can be seen in Fig. 9.

For purposes of comparison, we aggregated the agroclimatic regions and used the most suited slope values for winter cereals, since winter wheat dominates this category. If the SOS is neglected, as it did not demonstrate a significant trend in our study, the MAX_DOY parameter exhibits a steeper negative slope of approximately 2.5 days per decade in the two lower elevation intervals and 1 day per decade in the highest interval, as shown in Table 5. The EOS shows a good fit with ripening, except in the high elevation interval where it indicates an advance to an earlier DOY of 1.7 days per decade. Despite these slight differences, both types of observation indicate the same trend direction and magnitude. The reasons for these differences are: i) the parameters are defined differently, although they are closely related; ii) winter cereals also include other crops (e.g. winter barley and winter rye); iii) the start and therefore the length of the time series differ (1961–2021 vs. 1986–2020). Nevertheless, the overlap between the two studies is the greatest among existing literature in terms of research objectives, covered territory and crop type.

Regarding the productivity parameters, the significant positive median slope differences in SINT for spring cereals and in LINT for winter and spring cereals indicate that these parameters increased more in warmer regions than in colder regions during the observed period. Conversely, the significant

Tab. 5 Comparison of trends in selected phenological parameters of winter cereals (winter wheat) in relation to elevation above mean sea level (a.m.s.l.). All parameters exhibited a significant trend, except SOS (in italics).

Elevation interval a.m.s.l. AGC regions	Results Bartošová et al. (2025)		LSP observations	
		Days per decade		Days per decade
0–299 m VT, T1–T3, MT3	jointing	−4.5	*SOS*	*−0.8*
	heading	−3.3	MAX_DOY	−5.6
	ripening	−4.4	EOS	−4.5
300–499 m MT1, MT2, MT4	jointing	−6.9	*SOS*	*−0.8*
	heading	−3.6	MAX_DOY	−6.2
	ripening	−4.8	EOS	−4.2
> 500 m MCH, CH	jointing	−5.7	*SOS*	*−1.8*
	heading	−4.0	MAX_DOY	−5.1
	ripening	−3.3	EOS	−5.0

negative median for both SINT and LINT for fodder crops shows that productivity loss is smaller in colder regions during the observed period (as the slope is negative in the majority of agroclimatic regions).

Our first hypothesis was formulated as follows: "There are significant trends in LSP and productivity characteristics over the observed period." The results of the present analysis partially confirmed this. EOS and MAX_DOY were the only two parameters with a significant negative trend; however, this was only observed for cereals, rapeseed and fodder crops. Our study thus confirmed the existence of LSP trends and their direction over the observed 35-year period. At the same time, however, it showed that despite a significant trend in some LSP characteristics, the productivity parameters revealed negligible significance. The LSP of agricultural crops differs and should be considered in regional studies on crop productivity (Lobell and Gourdji 2012), land use and land cover changes (Zhang et al. 2019), and the impacts of global change on agriculture (Brown et al. 2012; Yuan et al. 2024) and vice LSP feedback to global change (Liu et al. 2017).

The results of the discussion also proved the validity of the second hypothesis: "Using high spatial resolution Landsat data and knowledge of the distribution of specific crops will enable us to observe differences in LSP and productivity trends between agroclimatic regions". Significant differences in trends in the LSP and productivity parameters were observed between the agroclimatic regions in 15 out of the 36 studied cases.

6. Conclusions

This study demonstrates the potential of long-term, high-resolution optical satellite data series for monitoring and analyzing trends in crop phenology and productivity at a regional scale. Using a 35-year Landsat time series, we evaluated four key phenological (SOS, EOS, LOS, MAX_DOY) and two productivity (SINT, LINT) parameters for six major crop types (winter cereals, spring cereals, winter rapeseed, fodder crops, sugar beetroot, and corn) in ten agro-climatic regions in Czechia. The methodology combined robust ground-based LAI measurements, advanced radiative transfer modeling (PROSAIL), machine learning-based LAI retrieval, and supervised crop classification to calculate dense LAI time series for each climatic region and crop. The annual LAI time series were then smoothed using a Savitzky-Golay filter and interpolated with RBF to produce daily profiles, from which phenological (SOS, EOS, LOS, MAX_DOY) and productivity (SINT, LINT) parameters were extracted using a threshold approach based on 25% of the annual LAI amplitude.

Accurate knowledge of crop types and their spatial distribution was essential for this study. Supervised classification of Landsat images using the SVM algorithm provided results with an overall accuracy of higher than 80% for all validated years. The achieved accuracy is comparable or better than other approaches in recent regional studies based on Landsat data. The phenology and productivity parameters in Czechia have shown different trends over the last four decades across climatic regions and crop types. While global vegetation studies often find a lengthening of the growing season due to earlier spring and later autumn, our analysis of six key crop types between 1986 and 2020 in Czechia tends to show only a significant negative shift of EOS and MAX-DOY – especially for winter and spring cereals, winter rapeseed (up to −0.7 days/year) and fodder crops (up to −1.6 days/year). For agricultural crops in general, EOS reflects the harvest date rather than natural senescence and is thus strongly related to MAX-DOY because the growing season is artificially terminated by harvest as the crop matures. Productivity trends varied by crop and climatic region, with SINT increasing significantly for spring cereals and sugar beetroot, while significant LINT trends were observed mainly for non-cereals in warmer regions. Approximately 40% of the crop and phenological/productivity parameter combinations show significant differences in trends between agro-climatic regions, with the shift in SOS and MAX_DOY for winter rapeseed occurring more rapidly in colder regions, while the shift in harvest dates and shortening of the season for corn and fodder crops is more pronounced in warmer regions. Comparison with phenological study based on altitude (Bartošová et al. 2025) confirmed similar directions and magnitudes of trends for winter cereals. Productivity parameters (SINT and LINT) for cereals increased more in warmer regions, while losses in fodder crops productivity were less pronounced in colder regions.

The study was based entirely on satellite data, and, to the authors' knowledge, it is unique in the level of detail of the performed analysis. In order to elaborate on differences in LSP and productivity trends between agroclimatic regions, detailed meteorological observations such as temperature and precipitation on a monthly or quarterly basis are necessary.

Acknowledgments

We would like to thank the Charles University Grant Agency for the support of this project in the form of grant number 293121: "Long-term development of phenological parameters of agricultural crops based on a 35-year time series of Landsat multispectral data". In addition, we would like to thank Gisat, Ltd. for providing the data and computing resources needed to successfully complete the project. We also appreciate the valuable comments and recommendations provided by the reviewers, which helped improve the quality of this manuscript.

Appendix 1 Trend slope values for individual phenological and productivity parameters derived over all combinations of climatic regions and crops of interest (W.C. = winter cereals, S.C. = spring cereals, W.R. = winter rapeseed, F.C. = fodder crops, S.B. = sugar beetroot, C. = corn). The slopes for SINT and LINT were calculated for values scaled by 0.0001.

	Crop	0:VT	1:T1	2:T2	3:T3	4:MT1	5:MT2	6:MT3	7:MT4	8:MT	9:MCH
Phenological parameters											
SOS	W.C.	−0.200	−0.100	−0.100	−0.100	−0.010	−0.068	0.040	−0.150	−0.190	−0.160
	S.C.	−0.300	−0.000	0.000	−0.100	−0.130	−0.500	−0.132	−0.053	0.020	−0.024
	W.R.	−0.200	−0.000	−0.300	**−0.300**	−0.100	−0.384	−0.175	−0.203	**−0.320**	−0.228
	F.C.	−0.200	0.030	−0.200	−0.300	−0.280	0.032	−0.056	−0.462	−0.210	−0.272
	S.B.	0.060	0.100	0.000	−0.200	−0.170	−0.029	0.104	0.128	−0.030	0.016
	C.	0.160	0.340	0.180	0.170	−0.090	0.298	0.293	0.242	0.396	0.114
EOS	W.C.	**−0.460**	**−0.370**	**−0.430**	**−0.600**	**−0.480**	**−0.410**	**−0.380**	**−0.370**	**−0.440**	**−0.550**
	S.C.	**−0.440**	**−0.350**	**−0.410**	−0.420	**−0.400**	−0.280	−0.350	**−0.480**	**−0.440**	−0.270
	W.R.	**−0.410**	−0.270	**−0.350**	**−0.480**	**−0.440**	**−0.440**	**−0.490**	**−0.380**	**−0.380**	−0.250
	F.C.	**−1.190**	**−1.630**	**−1.190**	**−0.750**	−1.050	−0.740	**−1.280**	**−0.810**	−0.200	**−1.140**
	S.B.	0.120	**−0.570**	−0.140	0.100	−0.150	0.040	−0.040	0.170	−0.300	0.030
	C.	−0.400	**−0.650**	−0.340	−0.210	−0.430	−0.130	0.080	−0.020	−0.190	−0.340
LOS	W.C.	−0.300	−0.300	−0.300	−0.500	−0.480	−0.338	−0.422	−0.220	−0.240	−0.392
	S.C.	−0.200	−0.300	−0.400	−0.300	−0.270	0.220	−0.220	−0.425	−0.460	−0.248
	W.R.	−0.300	−0.200	−0.100	−0.100	−0.340	−0.053	−0.316	−0.180	−0.060	−0.026
	F.C.	**−1.000**	**−1.700**	**−1.000**	−0.400	−0.770	−0.770	**−1.227**	−0.346	0.008	**−0.865**
	S.B.	0.060	**−0.700**	−0.100	0.280	0.025	0.069	−0.142	0.045	−0.270	0.017
	C.	−0.600	**−1.000**	−0.500	−0.400	−0.340	−0.425	−0.212	−0.266	−0.590	−0.450
MAX-DOY	W.C.	**−0.500**	**−0.500**	**−0.700**	**−0.700**	**−0.790**	**−0.599**	**−0.466**	**−0.457**	**−0.480**	**−0.536**
	S.C.	**−0.700**	**−0.600**	**−0.600**	**−0.400**	−0.200	**−0.669**	−0.441	**−0.525**	**−0.620**	−0.624
	W.R.	−0.200	**−0.600**	−0.500	**−0.500**	−0.460	**−0.595**	**−0.664**	**−0.659**	**−0.520**	**−0.515**
	F.C.	**−0.600**	**−0.800**	**−0.700**	**−0.400**	−0.610	**−0.563**	**−0.342**	−0.610	−0.340	−0.860
	S.B.	−0.500	−0.300	−0.300	−0.400	−0.480	−0.765	−0.019	−0.357	−0.090	−0.272
	C.	−0.200	0.090	−0.400	−0.200	0.181	0.491	0.044	**0.677**	0.732	0.414
Productivity parameters											
SINT	W.C.	−0.129	−0.103	−0.169	−0.151	−0.160	−0.156	−0.174	−0.117	−0.163	−0.152
	S.C.	**0.273**	**0.295**	**0.304**	**0.316**	**0.304**	**0.297**	**0.236**	0.167	0.152	**0.254**
	W.R.	−0.064	−0.006	0.091	0.050	−0.012	0.008	0.077	−0.039	−0.003	0.190
	F.C.	**−0.379**	**−0.419**	−0.299	−0.131	−0.236	−0.226	−0.185	−0.008	0.094	−0.165
	S.B.	0.133	0.170	**0.290**	**0.484**	**0.465**	**0.469**	0.262	0.191	0.115	**0.241**
	C.	0.041	0.050	0.056	0.036	0.153	0.092	0.077	0.101	−0.044	0.063
LINT	W.C.	0.123	0.172	0.101	0.160	0.158	0.071	0.084	0.102	0.033	0.018
	S.C.	0.133	0.083	0.060	0.103	0.123	0.059	0.196	0.095	0.005	0.006
	W.R.	0.205	0.272	0.246	**0.297**	**0.259**	0.110	0.133	0.145	0.070	0.162
	F.C.	**−0.419**	**−0.511**	**−0.361**	**−0.369**	−0.141	−0.306	−0.191	−0.299	−0.042	0.065
	S.B.	0.016	−0.053	0.078	0.120	**0.281**	0.142	0.229	0.125	0.087	−0.053
	C.	−0.108	**−0.237**	−0.136	−0.125	−0.054	−0.118	−0.082	−0.068	−0.066	−0.163

References

ARCSI GitHub. Available online: https://github.com/remotesensinginfo/arcsi (accessed on 20 June 2025).

Bartošová, L., Hájková, L., Pohanková, E., Možný, M., Balek, J., Zahradníček, P., Štěpánek, P., Dížková, P., Trnka, M., Žalud, Z. (2025): Differences in phenological term changes in field crops and wild plants – do they have the same response to climate change in Central Europe? International Journal of Biometeorology 69, 659–670, https://doi.org/10.1007/s00484-024-02846-8.

Brown, M. E., de Beurs, K. M., Marshall, M. (2012): Global phenological response to climate change in crop areas using satellite remote sensing of vegetation, humidity and temperature over 26 years. Remote Sensing of Environment 126, 174–183, https://doi.org/10.1016/j.rse.2012.08.009.

Campioli, M., Marchand, L. J., Zahnd, C., Zuccarini, P., McCormack, M. L., Landuyt, D., Lorer, E., Delpierre, N., Gričar, J., Vitasse, Y. (2025): Environmental Sensitivity and Impact of Climate Change on leaf-, wood- and root Phenology for the Overstory and Understory of Temperate Deciduous Forests. Current Forestry Reports 11: 1, https://doi.org/10.1007/s40725-024-00233-5.

Caparros-Santiago, J. A., Rodriguez-Galiano, V., Dash, J. (2021): Land surface phenology as indicator of global terrestrial ecosystem dynamics: A systematic review. ISPRS Journal of Photogrammetry and Remote Sensing 171, 330–347, https://doi.org/10.1016/j.isprsjprs.2020.11.019.

Chaves, E. D., Picoli, M. C. A., Sanches, I. D. (2020): Recent Applications of Landsat 8/OLI and Sentinel-2/MSI for Land Use and Land Cover Mapping: A Systematic Review. Remote Sensing 12(18): 3062, https://doi.org/10.3390/rs12183062.

Chmielewski, F.-M. (2013): Phenology in Agriculture and Horticulture. In Schwartz, M. (Ed.), Phenology: An Integrative Environmental Science. Dordrecht: Springer, 539–561, https://doi.org/10.1007/978-94-007-6925-0_29.

Claverie, M., Ju, J., Masek, J. G., Dungan, J. L., Vermote, E. F., Roger, J.-C., Skakun, S. V., Justice, C. (2018): The Harmonized Landsat and Sentinel-2 surface reflectance data set. Remote Sensing of Environment 219, 145–161, https://doi.org/10.1016/j.rse.2018.09.002.

Crhová, L., Kliegrová, S., Lipina, P., Tolasz, R., Valeriánová, A. (2022): Klimatologická ročenka České republiky 2021. Praha: Český hydrometeorologický ústav. Available online: https://info.chmi.cz/rocenka/meteo2021/ (accessed on 20 March 2025, in Czech).

de Beurs, K. M., Henebry, G. M. (2010): Spatio-Temporal Statistical Methods for Modelling Land Surface Phenology. In Hudson, I., Keatley, M. (Eds.), Phenological Research. Dordrecht: Springer, https://doi.org/10.1007/978-90-481-3335-2_9.

Decree No. 327/1998. Ministry of Agriculture of the Czech Republic. Available online: https://faolex.fao.org/docs/pdf/cze124894.pdf (accessed on 20 June 2025).

Dhakar, R., Sehgal, V. K., Chakraborty, D., Sahoo, R. N., Mukherjee, J. (2021): Field scale wheat LAI retrieval from multispectral Sentinel 2A-MSI and LandSat 8-OLI imagery: effect of atmospheric correction, image resolutions and inversion techniques. Geocarto International 36(18), 2044–2064, https://doi.org/10.1080/10106049.2019.1687591.

Dhillon, M. S., Dahms, T., Kübert-Flock, C., Liepa, A., Rummler, T., Arnault, J., Steffan-Dewenter, I., Ullmann, T. (2023a): Impact of STARFM on Crop Yield Predictions: Fusing MODIS with Landsat 5, 7, and 8 NDVIs in Bavaria Germany. Remote Sensing 15(6): 1651, https://doi.org/10.3390/rs15061651.

Dhillon, M. S., Kübert-Flock, C., Dahms, T., Rummler, T., Arnault, J., Steffan-Dewenter, I., Ullmann, T. (2023b): Evaluation of MODIS, Landsat 8 and Sentinel-2 Data for Accurate Crop Yield Predictions: A Case Study Using STARFM NDVI in Bavaria, Germany. Remote Sensing 15(7): 1830, https://doi.org/10.3390/rs15071830.

Dong, T., Liu, Jiangui, Qian, B., He, L., Liu, Jane, Wang, R., Jing, Q., Champagne, C., McNairn, H., Powers, J., Shi, Y., Chen, J. M., Shang, J. (2020): Estimating crop biomass using leaf area index derived from Landsat 8 and Sentinel-2 data. ISPRS Journal of Photogrammetry and Remote Sensing 168, 236–250, https://doi.org/10.1016/j.isprsjprs.2020.08.003.

dos Santos Luciano, A. C., Picoli, M. C. A., Duft, D. G., Rocha, J. V., Leal, M. R. L. V., le Maire, G. (2021): Empirical model for forecasting sugarcane yield on a local scale in Brazil using Landsat imagery and random forest algorithm. Computers and Electronics in Agriculture 184: 106063, https://doi.org/10.1016/j.compag.2021.106063.

Eklundh, L., Jönsson, P. (2015): TIMESAT: A Software Package for Time-Series Processing and Assessment of Vegetation Dynamics. In Kuenzer, C., Dech, S., Wagner, W. (Eds.), Remote Sensing Time Series. Remote Sensing and Digital Image Processing 22. Cham: Springer, https://doi.org/10.1007/978-3-319-15967-6_7.

Eklundh, L., Jönsson, P. (2016): TIMESAT for Processing Time-Series Data from Satellite Sensors for Land Surface Monitoring. In Ban, Y. (Ed.), Multitemporal Remote Sensing. Remote Sensing and Digital Image Processing 20. Cham: Springer, https://doi.org/10.1007/978-3-319-47037-5_9.

Fitchett, J. M., Grab, S. W., Thompson, D. I. (2015): Plant phenology and climate change: Progress in methodological approaches and application. Progress in Physical Geography 39(4), 460–482, https://doi.org/10.1177/0309133315578940.

Gao, F., Zhang, X. (2021): Mapping Crop Phenology in Near Real-Time Using Satellite Remote Sensing: Challenges and Opportunities. Journal of Remote Sensing 2021: 8379391, https://doi.org/10.34133/2021/8379391.

Gašparović, M., Pilaš, I., Radočaj, D., Dobrinić, D. (2024): Monitoring and Prediction of Land Surface Phenology Using Satellite Earth Observations – A Brief Review. Applied Sciences 14(24): 12020, https://doi.org/10.3390/app142412020.

Gitelson, A. A., Peng, Y., Masek, J. G., Rundquist, D. C., Verma, S., Suyker, A., Baker, J. M., Hatfield, J. L., Meyers, T. (2012): Remote estimation of crop gross primary production with Landsat data. Remote Sensing of Environment 121, 404–414, https://doi.org/10.1016/j.rse.2012.02.017.

Hajkova, L., Nekovar, J., Richterova, D., Koznarova, V., Sulovska, S., Vavra, A., Vozenilek, V. (2012): Phenological Observation in the Czech Republic – History and Present. Phenology and Climate Change. InTech, 71–100, https://doi.org/10.5772/35256.

Hanes, J. M., Liang, L., Morisette, J. T. (2014): Land Surface Phenology. In Hanes, J. M. (Ed.), Biophysical Applications of Satellite Remote Sensing. Springer Remote Sensing/Photogrammetry. Berlin, Heidelberg: Springer, https://doi.org/10.1007/978-3-642-25047-7_4.

Hassan, T., Gulzar, R., Hamid, M., Ahmad, R., Waza, S. A., Khuroo, A. A. (2023): Plant phenology shifts under climate warming: a systematic review of recent scientific literature. Environmental Monitoring and Assessment 196: 36, https://doi.org/10.1007/s10661-023-12190-w.

HR-VPP: User Manual. Available online: https://land.copernicus.eu/en/technical-library/product-user-manual-of-seasonal-trajectories/ (accessed on 20 June 2025).

Htitiou, A., Möller, M., Riedel, T., Beyer, F., Gerighausen, H. (2024): Towards Optimising the Derivation of Phenological Phases of Different Crop Types over Germany Using Satellite Image Time Series. Remote Sensing 16(17): 3183, https://doi.org/10.3390/rs16173183.

Huang, X., Fu, Y., Wang, J., Dong, J., Zheng, Y., Pan, B., Skakun, S., Yuan, W. (2022): High-Resolution Mapping of Winter Cereals in Europe by Time Series Landsat and Sentinel Images for 2016–2020. Remote Sensing 14(9): 2120, https://doi.org/10.3390/rs14092120.

Huang, X., Liu, J., Zhu, W., Atzberger, C., Liu, Q. (2019): The optimal threshold and vegetation index time series for retrieving crop phenology based on a modified dynamic threshold method. Remote Sensing 11(23): 2725, https://doi.org/10.3390/rs11232725.

Jeong, S.-J., Ho, C.-H., Gim, H.-J., Brown, M. E. (2011): Phenology shifts at start vs. end of growing season in temperate vegetation over the Northern Hemisphere for the period 1982–2008. Global Change Biology 17(7), 2385–2399, https://doi.org/10.1111/j.1365-2486.2011.02397.x.

Jönsson, P., Eklundh, L. (2004): TIMESAT – a program for analyzing time-series of satellite sensor data. Computers & Geosciences 30(8), 833–845, https://doi.org/10.1016/j.cageo.2004.05.006.

Kaspar, F., Zimmermann, K., Polte-Rudolf, C. (2014): An overview of the phenological observation network and the phenological database of Germany's national meteorological service (Deutscher Wetterdienst). Advances in Science and Research 11, 93–99, https://doi.org/10.5194/asr-11-93-2014.

Koch, E., Bruns, E., Chmielewski, F. M., Defila, C., Lipa, W., Menzel, A. (2007): Guidelines for plant phenological observations. World Climate Data and Monitoring Programme 1484, 1–41. Available online: https://library.wmo.int/viewer/51138/download?file=wmo-td_1484_en.pdf&type=pdf&navigator=1 (accessed on 20 June 2025).

Köppen climate classification. Available online: https://www.britannica.com/science/Koppen-climate-classification (accessed on 20 June 2025).

Lieth, H. (1974): Purposes of a Phenology Book. In Lieth, H. (Ed.), Phenology and Seasonality Modeling. Ecological Studies 8. Berlin, Heidelberg: Springer, https://doi.org/10.1007/978-3-642-51863-8_1.

Liu, F., Chen, Y., Shi, W., Zhang, S., Tao, F., Ge, Q. (2017): Influences of agricultural phenology dynamic on land surface biophysical process and climate feedback. Journal of Geographical Sciences 27, 1085–1099, https://doi.org/10.1007/s11442-017-1423-3.

Lobell, D. B., Gourdji, S. M. (2012): The Influence of Climate Change on Global Crop Productivity. Plant Physiology 160(4), 1686–1697, https://doi.org/10.1104/pp.112.208298.

Lu, L., Yu, L., Li, X., Gao, L., Bao, L., Chang, X., Gao, X., Cai, Z. (2025): Assessing Vegetation Canopy Growth Variations in Northeast China. Plants 14(1): 143, https://doi.org/10.3390/plants14010143.

Menzel, A. (2000): Trends in phenological phases in Europe between 1951 and 1996. International Journal of Biometeorology 44, 76–81, https://doi.org/10.1007/s004840000054.

Meroni, M., d'Andrimont, R., Vrieling, A., Fasbender, D., Lemoine, G., Rembold, F., Seguini, L., Verhegghen, A. (2021): Comparing land surface phenology of major European crops as derived from SAR and multispectral data of Sentinel-1 and -2. Remote Sensing of Environment 253: 112232, https://doi.org/10.1016/j.rse.2020.112232.

Michavila, M. A., Vicente-Serrano, S. M., Llovería, R. M., Cai, Z., Eklundh, L. (2024): Evaluación espacialmente continua de la dinámica de la fenología vegetal en España entre 1983 y 2020 a partir de imágenes de satélite. Cuadernos de Investigación Geográfica 50(1), 145–178, https://doi.org/10.18172/cig.5739.

Misra, G., Cawkwell, F., Wingler, A. (2020): Status of Phenological Research Using Sentinel-2 Data: A Review. Remote Sensing 12(17): 2760, https://doi.org/10.3390/rs12172760.

Mourad, R., Jaafar, H., Anderson, M., Gao, F. (2020): Assessment of Leaf Area Index Models Using Harmonized Landsat and Sentinel-2 Surface Reflectance Data over a Semi-Arid Irrigated Landscape. Remote Sensing 12(19): 3121, https://doi.org/10.3390/rs12193121.

Nord, E. A., Lynch, J. P. (2009): Plant phenology: a critical controller of soil resource acquisition. Journal of Experimental Botany 60(7), 1927–1937, https://doi.org/10.1093/jxb/erp018.

Olesen, J. E., Børgesen, C. D., Elsgaard, L., Palosuo, T., Rötter, R. P., Skjelvåg, A. O., Peltonen-Sainio, P., Börjesson, T., Trnka, M., Ewert, F., Siebert, S., Brisson, N., Eitzinger, J., van Asselt, E. D., Oberforster, M., van der Fels-Klerx, H. J. (2012): Changes in time of sowing, flowering and maturity of cereals in Europe under climate change. Food Additives & Contaminants: Part A 29(10), 1527–1542, https://doi.org/10.1080/19440049.2012.712060.

Pei, J., Tan, S., Zou, Y., Liao, C., He, Y., Wang, J., Huang, H., Wang, T., Tian, H., Fang, H., Wang, L., Huang, J. (2025): The role of phenology in crop yield prediction: Comparison of ground-based phenology and remotely sensed phenology. Agricultural and Forest Meteorology 361: 110340, https://doi.org/10.1016/j.agrformet.2024.110340.

Pluto-Kossakowska, J. (2021): Review on Multitemporal Classification Methods of Satellite Images for Crop and Arable Land Recognition. Agriculture 11(10): 999, https://doi.org/10.3390/agriculture11100999.

Qin, G., Wu, J., Li, C., Meng, Z. (2024): Comparison of the hybrid of radiative transfer model and machine learning methods in leaf area index of grassland mapping.

Theoretical and Applied Climatology 155, 2757–2773, https://doi.org/10.1007/s00704-023-04779-5.
Richter, K., Hank, T. B., Vuolo, F., Mauser, W., D'Urso, G. (2012): Optimal Exploitation of the Sentinel-2 Spectral Capabilities for Crop Leaf Area Index Mapping. Remote Sensing 4(3), 561–582, https://doi.org/10.3390/rs4030561.
Rodriguez-Galiano, V. F., Dash, J., Atkinson, P. M. (2015): Intercomparison of satellite sensor land surface phenology and ground phenology in Europe. Geophysical Research Letters 42(7), 2253–2260, https://doi.org/10.1002/2015GL063586.
Řezník, T., Pavelka, T., Herman, L., Lukas, V., Širůček, P., Leitgeb, Š., Leitner, F. (2020): Prediction of Yield Productivity Zones from Landsat 8 and Sentinel-2A/B and Their Evaluation Using Farm Machinery Measurements. Remote Sensing 12(12): 1917, https://doi.org/10.3390/rs12121917.
Schreier, J., Ghazaryan, G., Dubovyk, O. (2021): Crop-specific phenomapping by fusing Landsat and Sentinel data with MODIS time series. European Journal of Remote Sensing 54(sup1), 47–58, https://doi.org/10.1080/22797254.2020.1831969.
Shen, Y., Zhang, X., Yang, Z., Ye, Y., Wang, J., Gao, S., Liu, Y., Wang, W., Tran, K. H., Ju, J. (2023): Developing an operational algorithm for near-real-time monitoring of crop progress at field scales by fusing harmonized Landsat and Sentinel-2 time series with geostationary satellite observations. Remote Sensing of Environment 296: 113729, https://doi.org/10.1016/j.rse.2023.113729.
Sisheber, B., Marshall, M., Mengistu, D., Nelson, A. (2022): Tracking crop phenology in a highly dynamic landscape with knowledge-based Landsat–MODIS data fusion. International Journal of Applied Earth Observation and Geoinformation 106: 102670, https://doi.org/10.1016/j.jag.2021.102670.
Sisheber, B., Marshall, M., Mengistu, D., Nelson, A. (2023): Detecting the long-term spatiotemporal crop phenology changes in a highly fragmented agricultural landscape. Agricultural and Forest Meteorology 340: 109601, https://doi.org/10.1016/j.agrformet.2023.109601.
Skakun, S., Vermote, E., Franch, B., Roger, J.-C., Kussul, N., Ju, J., Masek, J. (2019): Winter Wheat Yield Assessment from Landsat 8 and Sentinel-2 Data: Incorporating Surface Reflectance, Through Phenological Fitting, into Regression Yield Models. Remote Sensing 11(15): 1768, https://doi.org/10.3390/rs11151768.
Sparks, T. H., Carey, P. D. (1995): The Responses of Species to Climate Over Two Centuries: An Analysis of the Marsham Phenological Record, 1736–1947. Journal of Ecology 83(2), 321–329, https://doi.org/10.2307/2261570.
Springer, T. L., Aiken, G. E. (2015): Harvest frequency effects on white clover forage biomass, quality, and theoretical ethanol yield. Biomass and Bioenergy 78, 1–5, https://doi.org/10.1016/j.biombioe.2015.04.003.
Tomíček, J., Mišurec, J., Lukeš, P. (2021): Prototyping a Generic Algorithm for Crop Parameter Retrieval across the Season Using Radiative Transfer Model Inversion and Sentinel-2 Satellite Observations. Remote Sensing 13(18): 3659, https://doi.org/10.3390/rs13183659.
Tomíček, J., Mišurec, J., Lukeš, P., Potůčková, M. (2022): Retrieval of Harmonized LAI Product of Agricultural Crops from Landsat OLI and Sentinel-2 MSI Time Series. Agriculture 12(12): 2080, https://doi.org/10.3390/agriculture12122080.
Unc, A., Altdorff, D., Abakumov, E., Adl, S., Baldursson, S., Bechtold, M., Cattani, D. J., Firbank, L. G., Grand, S., Guðjónsdóttir, M., Kallenbach, C., Kedir, A. J., Li, P., McKenzie, D. B., Misra, D., Nagano, H., Neher, D. A., Niemi, J., Oelbermann, M., Overgård Lehmann, J., Parsons, D., Quideau, S., Sharkhuu, A., Smreczak, B., Sorvali, J., Vallotton, J. D., Whalen, J. K., Young, E. H., Zhang, M., Borchard, N. (2021): Expansion of Agriculture in Northern Cold-Climate Regions: A Cross-Sectoral Perspective on Opportunities and Challenges. Frontiers in Sustainable Food Systems 5, https://doi.org/10.3389/fsufs.2021.663448.
Van Tricht, K., Degerickx, J., Gilliams, S., Zanaga, D., Battude, M., Grosu, A., Brombacher, J., Lesiv, M., Bayas, J. C. L., Karanam, S., Fritz, S., Becker-Reshef, I., Franch, B., Mollà-Bononad, B., Boogaard, H., Pratihast, A. K., Koetz, B., Szantoi, Z. (2023): WorldCereal: a dynamic open-source system for global-scale, seasonal, and reproducible crop and irrigation mapping. Earth System Science Data 15(12), 5491–5515, https://doi.org/10.5194/essd-15-5491-2023.
Webb, N., Nicholl, C., Wood, J., Potter, E. (2016): SunScan Manual, Version 3.3; Delta-T Devices Ltd.: Cambridge, UK, 1–82. Available online: https://delta-t.co.uk/wp-content/uploads/2017/02/SSI-UM_v3.3.pdf (accessed on 20 January 2025).
Wielgolaski, F.-E. (1974): Phenology in Agriculture. In Lieth, H. (Ed.), Phenology and Seasonality Modeling Studies 8. Berlin, Heidelberg: Springer, https://doi.org/10.1007/978-3-642-51863-8_31.
Wolanin, A., Camps-Valls, G., Gómez-Chova, L., Mateo-García, G., van der Tol, C., Zhang, Y., Guanter, L. (2019): Estimating crop primary productivity with Sentinel-2 and Landsat 8 using machine learning methods trained with radiative transfer simulations. Remote Sensing of Environment 225, 441–457, https://doi.org/10.1016/j.rse.2019.03.002.
Xu, J., Quackenbush, L. J., Volk, T. A., Im, J. (2022): Estimation of shrub willow biophysical parameters across time and space from Sentinel-2 and unmanned aerial system (UAS) data. Field Crops Research 287: 108655, https://doi.org/10.1016/j.fcr.2022.108655.
Yuan, X., Li, S., Chen, J., Yu, H., Yang, T., Wang, C., Huang, S., Chen, H., Ao, X. (2024): Impacts of Global Climate Change on Agricultural Production: A Comprehensive Review. Agronomy 14(7): 1360, https://doi.org/10.3390/agronomy14071360.
Zhang, H., Zhang, Y., Liu, K., Lan, S., Gao, T., Li, M. (2023): Winter wheat yield prediction using integrated Landsat 8 and Sentinel-2 vegetation index time-series data and machine learning algorithms. Computers and Electronics in Agriculture 213: 108250, https://doi.org/10.1016/j.compag.2023.108250.
Zhang, X., Liu, L., Henebry, G. M. (2019): Impacts of land cover and land use change on long-term trend of land surface phenology: a case study in agricultural ecosystems. Environmental Research Letters 14(4): 044020, https://doi.org/10.1088/1748-9326/ab04d2.
Zhang, X., Tan, B., Yu, Y. (2014): Interannual variations and trends in global land surface phenology derived

from enhanced vegetation index during 1982–2010. International Journal of Biometeorology 58, 547–564, https://doi.org/10.1007/s00484-014-0802-z.

Zhou, J., Jia, L., Menenti, M. (2015): Reconstruction of global MODIS NDVI time series: Performance of Harmonic ANalysis of Time Series (HANTS). Remote Sensing of Environment 163, 217–228, https://doi.org/10.1016/j.rse.2015.03.018.

Zhu, Z., Wang, S., Woodcock, C. E. (2015): Improvement and expansion of the Fmask algorithm: Cloud, cloud shadow, and snow detection for Landsats 4–7, 8, and Sentinel 2 images. Remote Sensing of Environment 159, 269–277, https://doi.org/10.1016/j.rse.2014.12.014.

Zhu, Z., Woodcock, C. E. (2012): Object-based cloud and cloud shadow detection in Landsat imagery. Remote Sensing of Environment 118, 83–94, https://doi.org/10.1016/j.rse.2011.10.028.